Received: December 10, 2020. Revised: February 4, 2021.

INASS

International Journal of
Intelligent Engineering & Systems

http://www.inass.org/

Coordinated Control of Battery Energy Storage System Based on Fuzzy Logic for Microgrid with Modified AC Coupling Configuration

Adhi Kusmantoro[1,2]* Ardyono Priyadi[1] Vita Lystianingrum Budiharto Putri[1] Mauridhi Hery Purnomo[1,3,4]

[1]*Department of Electrical Engineering, Institut Teknologi Sepuluh Nopember, Surabaya, Indonesia*
[4]*Department of Electrical Engineering, Universitas PGRI Semarang, Semarang, Indonesia*
[2]*Department of Computer Engineering, Institut Teknologi Sepuluh Nopember, Surabaya, Indonesia*
[3]*University Center of Excellence on Artificial Intelligence for Healtcare and Sociaety (UCE AIHeS), Indonesia*
* Corresponding author's Email: adhikusmantoro@mhs.ee.its.ac.id

Abstract: Microgrid systems are an excellent solution to increasing demand for electricity and are a great way to incorporate renewable energy sources into the electrical energy distribution system. To overcome the fluctuation of renewable energy (PV) based generation, an energy storage system using a battery (BESS) can be used. This paper proposes power management with a modified AC coupling configuration, and a BESS coordinated control strategy based on fuzzy logic. The AC coupling configuration in the microgrid system generally uses batteries to store excess power from the PV. In the proposed AC coupling configuration, two batteries are used, battery 1 (BESS 1) is used to store excess power of the PV array 1 (PVA1) via the inverter battery, while battery 2 (BESS 2) is used to store energy from the PV array 2 (PVA2)). In this microgrid system, PVA1 is connected to the network, so that the power generated by PVA1 is sent to the AC bus grid using a solar inverter. For two-way power flow on the grid and BESS, inverter batteries are used. The main focus of this article is the analysis of the impact of fuzzy logic (FLC) control strategy and PI control on BESS. When the PV is connected to the grid, control fuzzy logic (FLC) produces an overshoot of 4.73% and a settling time of 14.04 seconds lower than the PI control, overshoot 55.14% and settling time 26.29 seconds. The THD of the voltage and current in this mode is 0.06% and 11.08%. When the microgrid is in island mode, FLC produces an overshoot of 0.54% and a settling time of 13.78, while control PI produces an overshoot of 68.78% and a settling time of 38.11 seconds. The THD of voltage and current in island mode are 0.8% and 11.35%. Therefore, modified AC coupling configuration with fuzzy logic control (FLC) strategy can be used to serve residential loads.

Keywords: Coordinated control, Fuzzy logic controller, Battery inverter, PV array.

Nomenclature

P_{pv}: Output power PV
η_{pv}: PV generation efficiency
I_r: Solar radiation intensity
η_{pv}: PV generation efficiency
η_r: Efficiency of the PV module
η_{pc}: power conditioning efficiency
η_r: Module efficiency
β: Temperature coefficient
T_c: Cell temperature
T_{cr}: Reference cell temperature
T_a: Ambient temperature
T_{op}: Nominal operating cell temperature
I_{pvr}: Reference current at the nominal PV
K_i: Maximum temperature coefficient PV (A/ºK)
ΔT: Operating and nominal temperature
I_r: Radiation intensity on the module surface PV
I_{rn}: Nominal radiation intensity (1000 W/m^2)
A_{pv}: Total area of the PV array
P_{pvo}: Power of the PV array at STC
P_{pvp}: Output power of the PV array
K_T: Solar cell temperature coefficient (-37 x 10^{-31}/ºC)
$u(t)_P$: Active power output
$u(t)_Q$: Reactive power output
C: Battery capacity

 DOI: 10.22266/ijies2021.0430.45

t: Battery discharge time
k: Peukert coefficient
H: Rated discharge time
R: Represents the internal resistance
i: Represents the battery current (A)
i_f: Represents the filter current (A)
i_t: Represents the actual battery charge (Ah)
K: Represents the constant polarization (V/Ah)
V_b: Represents the battery voltage (V)
E_0: Represents the battery constant voltage (V)

1. Introduction

Use energy in the domestic sector in general is cosuminous, does not generate income-enhancing products or services. Furthermore, the electrical loads of households are typically extremely unpredictable, with low power. Solar power, which can be used as a versatile alternative to supply domestic electricity in Indonesia as a renewable source. In the isolated power grid areas (off grid) with the SHS (Solar Home System) program, the use of solar energy for households is typically done in Indonesia. When the power delivered by the SHS exceeds the power required by the charge, the SHS device uses a battery as an electrical energy stores [1].) Renewable energy generation has become more viable and cost-effective than fossil fuel power stations. By combining distributed energy resources at small scales, microgrids are implemented in the production of power at distribution voltage. The existence of unequaled and non-linear cargoes in the delivery system creates problems in the power efficiency of the Microgrid system [2]. The type of hybrid AC / DC microgrids is considered for higher energy conversion performance. In order to obtain better power sharing between the AC and DC subgrids, a coordinated IC (Interlink Converters) control strategy has been used, taking into account the charge state level (SOC) of the battery and the load shedding system as a last resort [3].

The study [4] proposed a coordinated control strategy based on fuzzy logic on batteries, to reduce the fluctuation of active power from the microgrid for network-connected operations and for island operations. The study results show that the proposed coordinated control is only able to reduce the fluctuation of active power in the microgrid for the control connected to the network, it is also seen that the SOC level of the battery greatly affects the load power. In study [5], it is proposed to control the flow of power to the load using a sliding mode controller and produce a fast dynamic response. This method is done by delaying the communication channel. However, this method has weaknesses, namely choosing the number of variables, the integral and variable derivatives, and limiting the analog component. In [6] the author proposes a drop control strategy in the battery converter. The proposed method serves as a decentralized droop control for load sharing, working for both grid-connected and island conditions. However, this method has not been able to solve the load power fluctuation quickly. Also in [7], a grid-connected PV-battery coordinated control strategy was proposed based on a virtual synchronous generator. The method used reduces the requirements for coordinated control systems and smooths the output power of the inverter, but is unable to work in island conditions. Another control strategy [8] is proposed for the integration of photovoltaic (PV) and batteries in a microgrid. This method works for islanding mode and grid-connected mode. The control strategy proposed by controlling the battery voltage, also used a bidirectional converter to connect the battery to the grid. This method aims to save excess energy on the grid to the battery. However, this method has a weakness, namely the battery energy is not able to serve the load when the system works in island mode. Another study [9] proposed an intelligent battery controller for standalone with PV and wind energy sources. This method aims to increase the generation capacity without increasing the battery capacity and to maintain the power needed by consumers. This method has the disadvantage of providing power to consumers when using low capacity batteries. Due to the discontinuous nature of renewable energy resources, the reliability of the microgrid system also decreases. Finally, an autonomous control strategy [10] was proposed for photovoltaic (PV) and battery packs operating in island mode with a drop control strategy in microgrid systems. The disadvantage of this method is that the battery is used only to supply power to the grid independently only during peak load periods. When the energy from the PV is cut off then the battery cannot supply power to the load for a long time. All studies have not oriented a battery capability strategy when the system operates in island mode, with renewable energy being cut off.

In this work we implemented a control strategy using a Fuzzy Logic controller in the energy storage system connected to the DC bus, with a modified microgrid AC coupling configuration, to achieve optimal AC bus power availability. Old model AC coupling configuration consisted of PV connected to the grid via solar inverter. In clear weather conditions, PV will provide maximum energy using MPPT (maximum power point tracking) to the solar inverter. Because the system is connected to the grid, the AC power generated by the solar inverter is supplied to

the AC grid bus [11, 12]. When there is excess power on the AC bus grid, the inverter battery will supply energy to the DC bus and from the DC bus energy is stored in the battery. When the power fluctuates in the grid, the energy stored by the battery is supplied to the grid from the DC bus using a battery inverter. The inverter battery in the AC coupling configuration works both ways [13]. The new model AC coupling configuration uses two PV arrays. PV array 1 is connected to the grid via a solar inverter, while the excess energy on the grid is stored in battery 1 (BESS 1). PV array 2 is used to charge battery 2 (BESS 2) using a boost converter. Battery 2 is used to overcome the change in power from battery 1. Battery 1 and battery 2 in this work is called a battery energy storage system (BESS) which is connected to the DC bus [14]. With this method, the availability of battery power for the power requirements of the AC bus can be more fulfilled, when compared to charging the battery through excess PV power on the AC bus. In the end, the fuzzy logic controller works to regulate the energy flow of battery 1 and battery 2 to the grid and regulate battery charge 1 from the excess energy on the grid. The controller stabilizes the DC bus voltage and supplies power to the network at a stable value. The proposed system can work in grid-connected mode and island mode.

After this introduction, we organize our work as in section 2: Model and description of the proposed PV system. Part 3: Explanation of power flow and control grid connected PV system. Part 4: Explanation of the solar inverter used. Section 5: Explanation of the battery model used. Section 6: Explanation of battery control strategy and control design using fuzzy logic, with grid and island connected mode. Section 7: Explanation of work results and discussion. In section 8: the conclusion of the work that has been done.

2. PV system

2.1 PV potential

Power performance of a PV array is dependent on solar irradiance and ambient temperature [15]. The power output in this model is determined as

$$P_{pv} = \eta_{pv} \times A_{pv} \times I_r \quad (1)$$

Based on Eq. (1), the output power of PV (P_{pv}) depends on the PV generation efficiency (η_{pv}), the cross-sectional area of PV (A_{pv}), and the amount of solar radiation intensity (I_r). Meanwhile, the PV generation efficiency (η_{pv}) is influenced by the efficiency of the PV module (η_r) and the power conditioning efficiency (η_{pc}). Module efficiency (η_r) depends on the temperature coefficient (β) and the difference between cell temperature (T_c) and reference cell temperature (T_{cr}), Eq. (2).

$$\eta_{pv} = n_r \times \eta_{pc}[1 - \beta(T_c - T_{cr})] \quad (2)$$

The temperature coefficient (β) is 0.004 - 0.006 / ºC. The amount of reference cell temperature (T_{cr}) is strongly influenced by changes in ambient temperature (T_a), still, according to Eq. (3). Meanwhile, the effect of solar radiation intensity (I_r) in this equation also depends on the nominal operating cell temperature (T_{op}).

$$T_{cr} = T_a + \left\{\frac{T_{op}-20}{800}\right\} \times I_r \quad (3)$$

2.2 Modeling PV

The P-N junction semiconductor, which is the solar array building block, can generate electricity due to the photovoltaic effect. In series-parallel configuration PV cells are interconnected to form a PV array [16]. Using single diode model, I-V characteristics of PV cells can be derived. In this model there is a shunt resistance (R_{sh}) connected in parallel [17]. Solar cells are non-linear components which can be shown in Fig. 1 as a model of current sources. The value of the shunt resistance (R_{sh}) is usually very large, and the value of the series resistance (R_s) is very small, so the analysis is negligible. PV cells are grouped into large units called PV modules that are also connected to form PV arrays or PV generators in a parallel series configuration [18].

By using Kirchoff's current law in the equivalent circuit of Fig. 1, the current equation for the PV module terminals is obtained as follows

$$I_T = I_{pv} - I_D \quad (4)$$

where I_T, I_D, I_{pv} are the currents at the terminal of

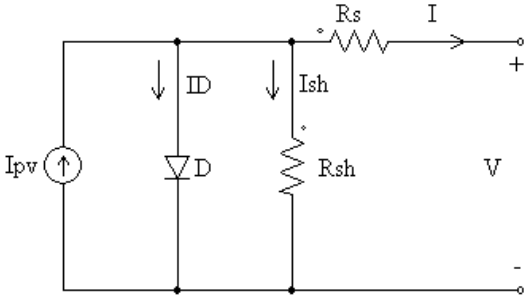

Figure. 1 Equivalent circuit of the PV cell one-diode model

the PV module, the diode currents, and the currents generated by the PV cells. The current I_{pv} can be expressed by the following equation

$$I_{pv} = \left(I_{pvr} + K_i \Delta T\right) \frac{I_r}{I_{rn}} \quad (5)$$

where I_{pvr}, K_i, ΔT, I_r, I_{rn} is the reference current at the nominal conditions generated by PV due to solar radiation, the maximum temperature coefficient of the cell current in the PV module (A/ºK), the difference between the operating temperature and the nominal temperature, the radiation intensity on the module surface PV, and nominal radiation intensity (1000 W/m^2). The amount of current I_{pv} depends on the difference in temperature and the intensity of solar radiation. By considering the PV cell as an ideal diode, it can be expressed by the equation

$$I_D = I_0 \left\{ e^{\left(\frac{V+R_S I}{\alpha V_t}\right)} - 1 \right\} \quad (6)$$

where I_0, V_t is the PV cell diode saturation current when there is no solar radiation, and the PV cell thermal voltage. This thermal stress is influenced by the number of PV cells connected in series, so it is mathematically expressed by the equation

$$V_t = \frac{N_s K T}{q} \quad (7)$$

where N_s, K, q, α is the number of series connected PV cells, Boltzmann's constant (1.3806 x 10^{-23} J/K), electron charge (1.602 x 10^{-19} C), operating temperature (K), and ideal constant diode with a value between 1 and 1.5. By substituting Eq. (3) to equation 1, the current magnitude at the PV module terminal is

$$I_T = I_{pv} - I_0 \left\{ e^{\left(\frac{V+R_S I}{\alpha V_t}\right)} - 1 \right\} \quad (8)$$

The current flowing in the resistance R_{sh} can be expressed mathematically by the following equation

$$I_{sh} = \frac{V+R_S I_T}{R_{sh}} \quad (9)$$

Based on the PV cell equivalent circuit, the total current at the PV module terminal is expressed by the following equation

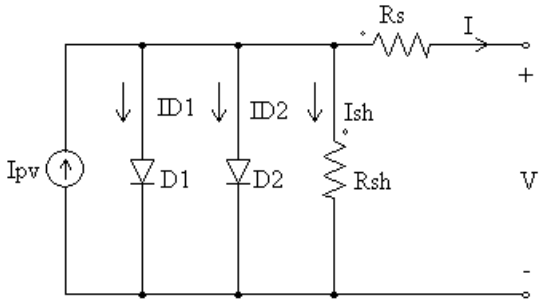

Figure. 2 Double diode PV model

$$I_T = I_{pv} - I_0 \left\{ e^{\left(\frac{V+R_S I}{\alpha V_t}\right)} - 1 \right\} - \frac{V+R_S I_T}{R_{sh}} \quad (10)$$

PV cell output current can be represented using two diode model [19]:

$$I_T = I_{pv} - I_{D1} - I_{D2} - \left\{\frac{V+R_S I}{R_{sh}}\right\} \quad (11)$$

For the arrangement of PV cells connected in series and parallel, each will provide the output voltage and output current, so that it is mathematically expressed by the following equation

$$R_{SP} = \frac{N_s}{N_p} \times R_S \quad (12)$$

$$I_{pvP} = N_p \times I_{pv} \quad (13)$$

$$I_T = N_p \times I_P \quad (14)$$

$$V_T = N_s \times V \quad (15)$$

Eqs. (12) – (15) state the total value of series resistance, PV current, PV module terminal current, and PV module terminal voltage based on the number of PV cells connected in series and parallel.

2.3 PV system capacity

The PV power (PPV), based on residential homes requirements and total daily solar (H) energy in KW /m^2/day, is computed to meet the required daily charge E_1. The efficiency of photovoltaic (PV) is low, this is due to the internal influence of series and shunt resistance and the effect of recombination in photovoltaics. Efficiency of other device parts including output of the charging controller, DC-AC performance (inverter) and output of the battery storage [20].

The total area of the PV array $\left(A_{pv}\right)$ requested may be determined as follows according to the above parameters.

Table 1. Electrical characteristic of PV panel

Parameter	Values
Maximum Power (P_{max})	250 Wp
Voltage at Maximum Power (V_{mpp})	30.61 V
Current at Maximum Power (I_{mpp})	8.17 A
Open Circuit Voltage (V_{oc})	38.06 V
Short Circuit Current (I_{sc})	8.54 A
Temperature Coefficient of (P_{max})	-0.46 %/°C
Temperature Coefficient of (V_{oc})	-0.31 %/°C
Temperature Coefficient of (I_{sc})	0.015 %/°C

$$A_{pv} = \frac{E_1}{H \times T_c \times \eta_{PV} \times \eta_{inv} \times \eta_c \times \eta_b} \quad (16)$$

The PV array of peak outputs can be measured according to the normal solar radiation H_{sc} of 1000 W/m^2:

$$P_{pv} = A_{pv} \times H_{sc} \times \eta_{pv} \quad (17)$$

In order to measure the PV array maximum power, Eqs. (16) and (17) can be used. The DC energy provided by the PV system mainly depends on various factors, such as the standard test conditions for PV peak power (STC), solar radiation and cell temperature. As is seen in the simple model:

$$P_{pvo} = P_{pvp} \times \left\{\frac{I_r}{I_{rn}}\right\} \times [1 + K_T(T_c - T_{cr})] \quad (18)$$

were P_{pvo}, P_{pvp}, K_T is the power of the PV array at STC, the output power of the PV array, the monocrystalline and polycrystalline Si solar cell temperature coefficient (-37 x 10^{-31}/ºC) [21]:

$$T_c = T_a + (0{,}0256 \times I_r) \quad (19)$$

where T_a is the ambient temperature.
In this work, we used the PV module Solaria S6M2G250 (monocrystalline) characterized by the technical parameters listed in the following Table 1. This PV module has 60 cells number.

3. Grid connected PV

The PV network mathematical model connected to the grid would also involve both the PV array and the inverter mathematical model. Fig. 3 defines the PV network connected to the grid and the controller. PV is the source and generates solar energy electricity here. The PV linked the grid through the inverter, the LC filter and the PCC. The inverter turns the DC input into AC and is supplied with the LC filter. A continuous power flow parameter for both the regular and abnormal conditions is the main objective of the grid-related PV topology. Using grid parameters, the

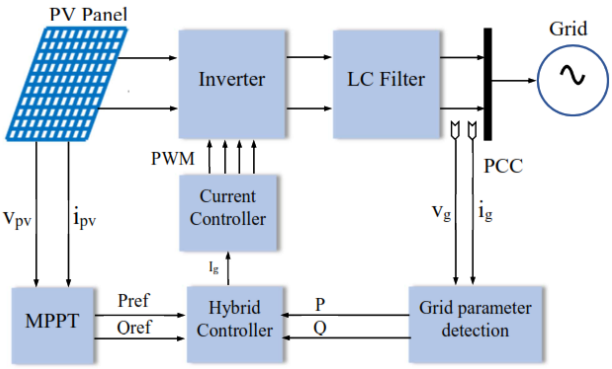

Figure. 3 Block diagram of the grid connected PV system

proposed control technique would produce power pulses of the inverter [22].

The LC filter in solar inverter is used to restrict the higher order harmonics from the switching behavior of the inverter as seen in the Fig. 3. Hence, the method on the ac-side can be explained in the following equation, ignoring all of the filter losses.

$$\frac{di_g(t)}{dt} = \frac{V_{inv}(t)}{L} - C_f \frac{d^2V_g(t)}{dt^2} - \frac{V_g(t)}{L} \quad (20)$$

Where i_g is a grid current injected, v_g is the grid voltage and vinvis the output voltage of the inverter. Grid parameters like voltage and current are important in determining the grid side PQ used to calculate the grid's current, active and reactive capacity. By using the following equations the active and reactive power supplied in the grid was determined. The following are Eqs. (21) and (22).

$$P = \frac{1}{2}\{v_g^d \times i_g^d\} \quad (21)$$

$$Q = -\frac{1}{2}\{v_g^d \times i_g^d\} \quad (22)$$

Where Δp and Δq are a dq-rotating synchronous reference frame of the grid voltage and current. P and Q are both active and reactive power. The PQ problem can be defined by measuring the error between the real grid side parameters and the reference power values of the PV network. For the estimation of power value, the PV system uses the MPPT (Maximum Power Point Tracking).
In the following eqs the error calculation is specified Eqs. (23) and (24), respectively.

$$\Delta P = [P(act) - P(ref)] \quad (23)$$

$$\Delta Q = [Q(act) - Q(ref)] \quad (24)$$

The error values of active and sensitive power are ΔP and ΔQ. The real active and reactive force are $P(act)$

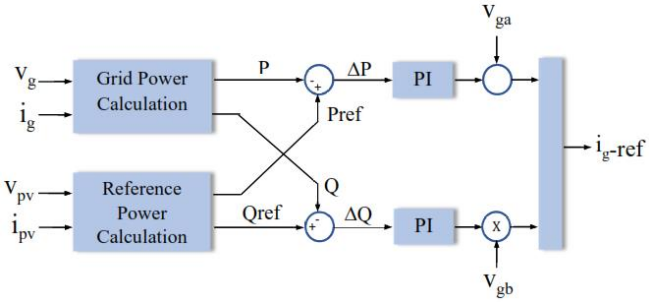

Figure. 4 Controller diagram of the grid connected PV system

and $Q(act)$. The active and the reactive power relation are $P(ref)$ and $Q(ref)$. The PI controller mentioned in Fig. 4 is allowed for error values. The PI controller's output performance is shown mathematically in the following Eqs. (25) and (26), respectively.

$$u(t)_P = \Delta P(t) \times \left[K_P + K_I \int_0^t dt\right] \quad (25)$$

$$u(t)_Q = \Delta Q(t) \times \left[K_P + K_I \int_0^t dt\right] \quad (26)$$

Where $u(t)_P$ and $u(t)_Q$ are the active power and reactive power output property of the PI controller, the proportional gain is the K_P and the integral gain is the K_I.The existing reference values for the $\alpha\beta$ method are calculated accordingly [23].

$$i_g^{\alpha}(ref) = \frac{2\left(v_g^{\alpha} P(ref) + v_g^{\beta} Q(ref)\right)}{\left(v_g^{\alpha}\right)^2 + \left(v_g^{\beta}\right)^2} \quad (27)$$

$$i_g^{\beta}(ref) = \frac{2\left(v_g^{\beta} P(ref) + v_g^{\alpha} Q(ref)\right)}{\left(v_g^{\alpha}\right)^2 + \left(v_g^{\beta}\right)^2} \quad (28)$$

In cases where $i_g^{\alpha}(ref)$ and i_g^{β} are the $\alpha\beta$ system reference grid current, $v_g^{\alpha}(ref)$ and $v_g^{\beta}(ref)$ are the $\alpha\beta$ system grid voltage.

4. Solar inverter

The efficiency of a photovoltaic system is dependent on more than a factor such as the inverter output. ICA Inverter is the inverter used in this study and is nearest to realistic implementations. Actually, a DC/AC inverter converts the current of the DC provided by the PV array to the current of the AC. The efficiency of this method can be expressed by

$$\eta(t) = \frac{(P_{in}(t) - P_{loss}(t))}{P_{in}(t)} \quad (29)$$

Where $P_{in}(t)$ is the PV array input and $P_{loss}(t)$ is the loss of converting power. In order to model and characterize the inverter as a general relationship of the inverter efficiency and PV power is established

$$\eta_{inv} = AP_{pv}^n + B, P_{pv} \leq N \quad (30)$$

$$\eta_{inv} = AP_{pv}^n + B, P_{pv} \geq N \quad (31)$$

The method used in this analysis therefore model an inverter based on the principle of correlation between the manufacturer's curve (characteristic curve) and the experimental results. In terms of inverter capacity, Eqs. (30) and (31) are generally applicable to this type of inverter. They can, however, also be used and used on many other inverters. The consumer wants, therefore, to obtain a more reliable inverter model, new equations for certain types of inverters [24].

The Low Pass Filter First Order (LPF) is typically used to obtain the average active and reactive power value. However, due to the large filter-time value, the transient response of the device becomes sluggish. In order to enhance the transient response of the various research community, SOGI is used with the first order low pass filter [25].

$$G_f = \left\{\frac{2\zeta\omega_f s}{d}\right\} \times \left\{\frac{\omega_n}{d}\right\} \quad (32)$$

where d is the denominator of the low pass filter equation, first order $(d = s^2 + 2\zeta\omega s + \omega^2)$. In order to synchronize the inverter current with the grid voltage, the phase angle of the modulating signal (Vm) varies by the solar irradiance and temperature point. For a certain range of temperature and irradiation level the correct phase angle must be defined. The phase angle of Vm in the developed model changes automatically to the right value, depending on the cell temperature range [26].

5. Battery energy storage system

Batteries are the cornerstone of inverters, as the solar PV system can't supply the energy during the absence of the sun (night time) without energy storage. The battery model works in two ways loading and unloading. If the current is positive and the current discharge mode is negative, the battery is charged. In case of grid outage or when the device is running alone, batteries are used for stocking excess PV power. They also help load when the power of the PV is below the demand for load. [27]. The life of the battery depends on the system's energy consumption rate. The Peukert Law is generally used for estimating battery discharge in light of the battery's

nonlinear characteristics. The law of Peukert is mentioned mathematically as

$$t_{disc} = H\left\{\frac{C}{IH}\right\}^{k} \quad (33)$$

Where I, C, t, k, H, is the current drawn, battery capacity (ampere hour value), battery discharge time, peukert coefficient, and rated discharge time. The coefficient of Peukert is an empirical value determinable by formula

$$k = \frac{logT_2 - logT_1}{logI_1 - logI_2} \quad (34)$$

where T_1 and T_2 are the corresponding discharge duration, and I_1 and I_2 are the two discharge current rates. After such recharge cycles, the value of k should be accessed [28].

$$t_{charg} = \frac{Ah}{I_{charg}} \quad (35)$$

Lead Acid battery model charging and discharging characteristics must be implemented mathematically which follows the following equation

$$v_b = E_0 - iR - \left[K\frac{Q}{Q - i_t}\left(i_t + i_f\right)\right] \quad (36)$$

where R represents the internal resistance, i represents the battery current (A), i_f represents the filter current (A), i_t represents the actual battery charge (Ah), Q represents the battery capacity (Ah), K represents the constant polarization (V/Ah), V_b represents the battery voltage (V), E_0 represents the battery constant voltage (V). The SOC on a battery can use the coulomb equation [29].

$$SOC(t) = \left\{SOC(t_0) - \left(\frac{\int i_b(t)dt}{Q_N}\right)\right\} \quad (37)$$

The SOC of the battery must work in a safe range and can cause permanent damage to the battery if they are taken out of a safe range. The secure operating range of the SOC is set by the above and below limit of 80 % and 20% respectively [30].

6. Proposed modified AC coupling

The system proposed in the design of the microgrid system uses a new configuration, namely modification of the AC coupling configuration which includes two stages as follows:

Phase I - Development of the AC coupling configuration with a battery as energy storage through a DC-DC converter and PV array 2 (PVA2). The model development consists of several components, namely PV array, battery storage, solar inverter, battery converter (battery inverter), boost converter and control strategy. The control strategy uses control coordination on the PV array 1 (PVA1) connected to the grid via an inverter and a battery connected to the DC bus.

Phase II - Development of a control strategy based on fuzzy logic on the BESS side (battery 1 and battery 2), in regulating the power flow to the DC bus. Charging battery 1 from excess power of PV 1 (PVA1) array via inverter battery and charging battery 2 from PV panel 2 (PVA2) via DC-DC converter.

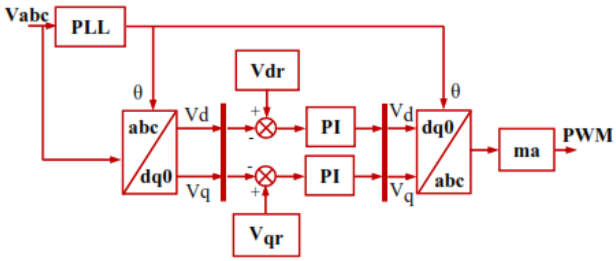

Figure. 5 Inverter control strategy

6.1 Inverter control strategy

The control loop for the PQ controller strategy is shown in Fig. 5. The model is based upon a synchronous reference device and varies the angle of firing for the various switches to ensure constant voltage and frequency in the output of the inverter. There is separate regulation of active power and reactive power. The lock loop phasing unit (PLL) computes the reference angle of the synchronous frame. The voltage at the inverter terminal is divided into active (Vd) and reactive (Vq) components by "abc to dq0" transformation. To change its shape it transfer the difference from the decomposed sum to the reference quantity over the PI controller. In addition, Vd, Vq and V0 (null sequence) are positioned by the transformation from dq0 to abc with the reference PLL angle, which generates a pulse loop by the use of PWM.

6.2 DC bus power droop control

The DC bus power droop control is shown in Fig. 6. When battery source 1 meets the demand for load power, then battery 1 is operating providing a constant power source to the DC bus (PB1). When the output power of battery 1 and load power increases, resulting in battery 1 supply power being smaller than the load power demand, the DC bus

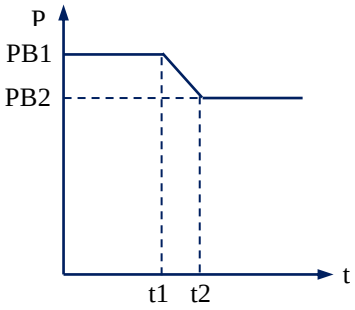

Figure. 6 The principle of droop control with a battery source on the DC Bus

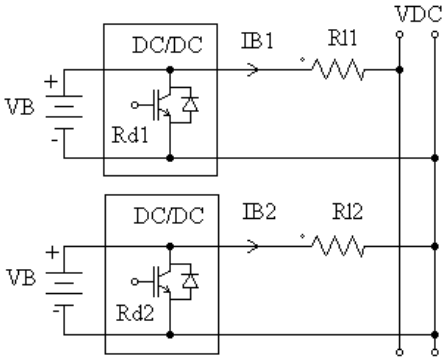

Figure. 7 Parallel distribution of batteries with drop control

power will decrease. In this condition the DC bus power will drop towards the threshold power from battery source 2 (PB2). Battery 2 will be connected as constant power source to the DC bus.

In DC power droop control with two battery power sources distributed in parallel providing power to the DC bus. Based on Fig. 7, the equation for the droop control strategy can be derived as follows

$$V_{DC} = V_B - R_{d1}I_{B1} - R_{l1}I_{B1} \tag{38}$$

$$V_{DC} = V_B - R_{d2}I_{B2} - R_{l2}I_{B2} \tag{39}$$

Combining Eqs. (1) and (2) is obtained

$$\frac{I_{B1}}{I_{B2}} = \frac{R_{d2}+R_{l2}}{R_{d1}+R_{l1}} \tag{40}$$

where V_{DC}, V_B, K_1, K_2, I_{B1}, I_{B2}, R_{l1}, R_{l2} are the DC bus voltage, battery voltage, converter virtual resistance 1, converter virtual resistance 2, battery current 1, battery current 2, battery line resistance 1, line resistance from battery 2. It can be seen from Eq. (40) that the output current of each battery is inversely proportional to the sum of the virtual converter resistance and the line resistance to the DC bus. It is known that the two battery sources have the same capacity, and for the needs of the virtual converter resistance and line resistance are considered the same. Therefore, coordination must be done in regulating battery currents.

$$\frac{R_{d2}}{R_{d1}} \neq \frac{R_{l2}}{R_{l1}} \tag{41}$$

There is a circulating current in the network because the output current from the battery source is distributed differently.

$$\frac{I_{B1}}{I_{B2}} \neq \frac{R_{d1}}{R_{d2}} \tag{42}$$

From the analysis of the above equation, the output power of battery 1 and battery 2 is different due to the different parameters of the battery source and the distributed path. When the battery parameter is low, circulating currents occur and the stability of the DC bus power is affected. Therefore, a control strategy using fuzzy logic is used in this study.

6.3 Battery control strategy

To provide adequate power flow and protection for the equipment, a modified version of the charge controller is shown in Fig. 7. BESS (battery energy storage system) consists of battery 1 and battery 2. PVA2 energy source and PVA1 excess power as a source of electrical energy for the battery. The secondary PVA2 energy source has generated energy to increase the reliability of the DC bus system without increasing the size of the battery bank. The system proposed in this research, PVA1 acts as the main energy source. Based on the load energy demand and the energy that has been generated, the battery can be in charge or discharge mode. If a battery connected to the primary source is unable to provide energy to the DC bus, the secondary energy source provides the energy needed for the load. Since the two energy sources are in sync with battery 1 and battery 2, all of the energy generated is used to increase the AC power capacity of the Bus. Fig. 8 shows the algorithm for charging, discharging the battery, floating state, and the operating system using four switches connected to the battery bank. When the energy produced by PVA1 decreases and the SOC of the battery is greater than the reference value, switch S2 is closed and battery bank 1 is connected to the DC Bus. When the energy stored in battery 1 is less than the predetermined value, switches S3 and S4 are closed and battery bank 2 is connected to the DC Bus. In this case the energy supplied by the secondary energy source (PVA2) to the battery is maintained charging, discharging or in a floating state based on the energy supplied from the source to the battery bank 2 and the energy supplied to the load. The

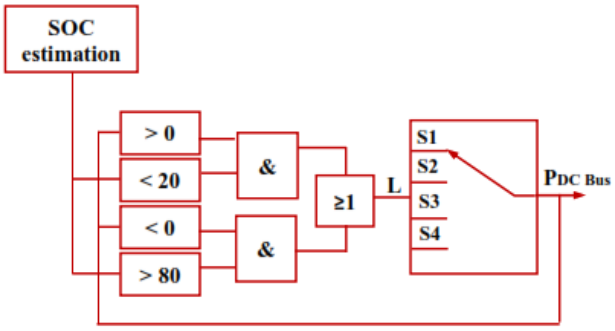

Figure. 7 Battery control operation 1 and 2

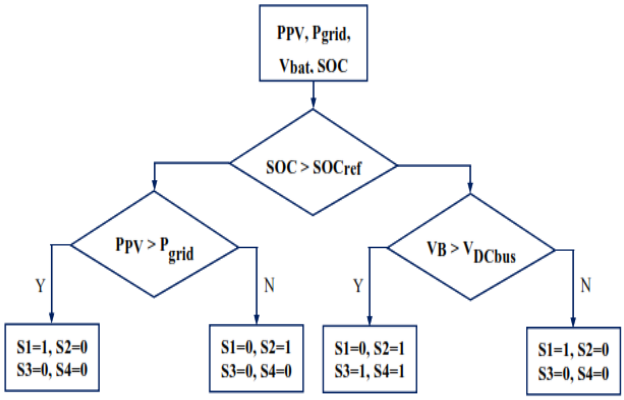

Figure. 8 Battery control operation algorithm

Table 2. Battery control operation

Battery SOC	$P_{DC\ Bus}$	S
> 80 %	> 0	0
> 80 %	< 0	S2
< 20 %	> 0	S1
< 20 %	< 0	S3,S4

voltage of each battery bank is served with minimum SOC conditions, so the voltage of each battery bank is low. So that the two banks serve in series with switches S1 and S4 closed. When the SOC of the battery bank is getting low, the battery bank cannot provide the required voltage, all switches are open and unable to serve the load.

6.4 Battery control with fuzzy logic

The coordinated control strategy is to determine the set points of the batteries that can be delivered. The objectives of the coordinated control are,

1) Stabilizes the microgrid output power in network-connected mode.
2) Maintain the voltage and frequency level in island mode.

6.4.1. Grid connected mode

In grid-connected mode, the microgrid frequency is closely linked to the buc AC grid. The battery will be charged when the charge level is lower than the

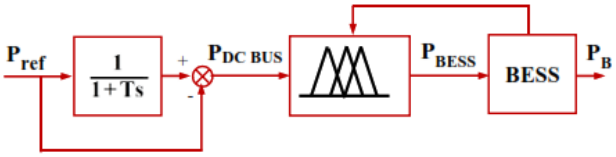

Figure. 9 Control for grid connected mode.

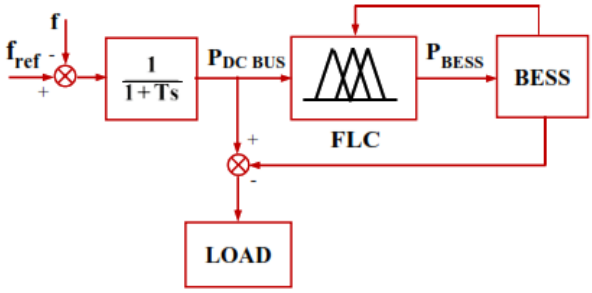

Figure. 10 Island mode control

preset threshold (SOC < 20%). In this design battery 1 and battery 2 are called the battery energy storage system (BESS). As shown in Fig. 8, reference the AC bus network active power output (P_{ref}) as fuzzy logic controller (FLC) input or $P_{DC\ Bus}$ input, to keep SOC BESS above a certain level and reduce fluctuation. Another input of FLC is SOC.

6.4.2. Island mode

The controller for the island operation is illustrated in Fig. 10. In this mode, microgrid frequency quality depends on the battery inverter. In this research, BESS plays a role in secondary control operation (battery inverter). During this period, BESS responds and energizes very quickly Table 4 shows the battery parameters. The power required by the load depends on the power on the DC bus or the SOC of the battery. The output frequency of the inverter battery is controlled based on the reference frequency (f_{ref}).

6.4.3. Design of fuzzy logic controller

As already explained, the fuzzy logic controller adjusts the active power of BESS based on SOC and DC Bus input active power for the condition of the PV connected to the network. When island conditions, the fuzzy logic controller adjusts the active power output from BESS based on the SOC and active power commands for reference frequency control. The FLC control strategy can be explained as follows

$$P_{BESS}\min \leq P_{BESS} \leq P_{BESS}max \quad (43)$$

$$SOC_{min} \leq SOC \leq SOC_{max} \quad (44)$$

$$P_{BESS} = fFLC(P_{DC\ Bus}, SOC) \quad (45)$$

Table 3. Fuzzy rules

SOC \ $P_{DC\ BUS}$	NH	NM	NL	ZE	PL	PM	PH
NH	NH	NH	NH	NM	NM	NL	ZE
NL	NH	NH	NM	NM	NL	ZE	PL
ZE	NM	NM	NL	ZE	PL	PM	PM
PL	NL	ZE	PL	PM	PM	PH	PH
PH	ZE	PL	PM	PM	PH	PH	PH

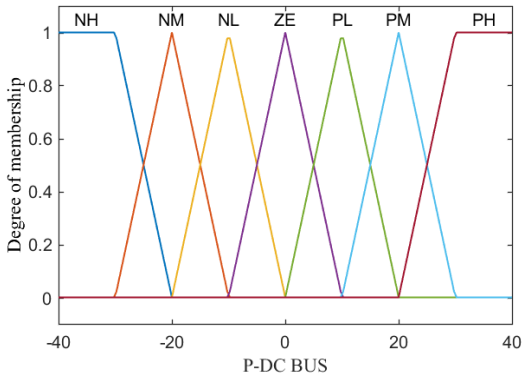

(a)

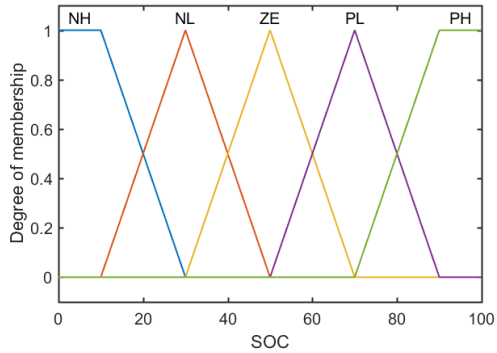

(b)

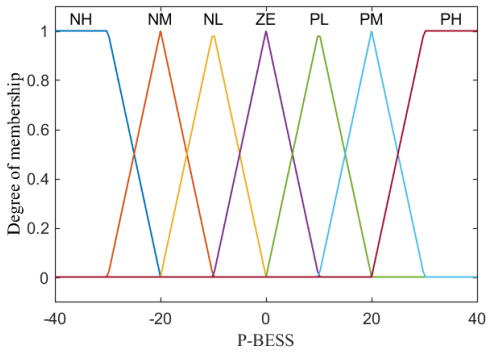

(c)

Figure. 11 Battery control memberships functions: (a) $P_{DC\ BUS}$ memberships functions, (b) SOC memberships functions, and (c) P_{BESS} memberships functions

Triangular membership function is a combination of two lines or linear. This membership function is determined by 3 parameters, namely {a, b, c} by following the rules in Eq. (46). The parameters {a, b, c} where a < b <c determine the x coordinates of the three angles of the triangle membership function.

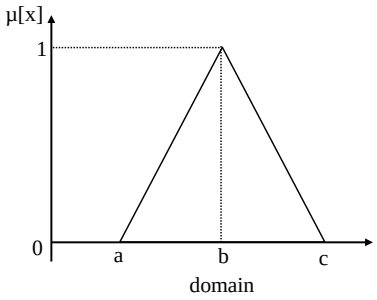

Figure. 12 Triangular memberships functions

Table 4. Parameters of the battery

Parameter	Value
Capacity per cell	100 Ah
Nominal Voltage	12 V
Total cells in series	4
Total row of cells in series	2
Total capacity BESS 1	200 Ah
Total capacity BESS 2	200 Ah
Total Voltage	48 V
Total Power	19,2 kWh

$$\mu(x) = \max(\min\left(\frac{x-a}{b-a}, \frac{c-x}{c-b}\right), 0) \qquad (46)$$

Inputs and outputs on the FLC have a membership function. The SOC input has five membership functions, namely Negative High (NH), Negative Low (NL), zero (ZE), Positive Low (PL) and Positive High (PH). For $P_{DC\ Bus}$ input there are seven membership functions, namely Negative High (NH), Negative Medium (NM), Negative Low (NL), zero (ZE), Positive Low (PL), Positive Medium (PM), Positive High (PH). P_{BESS} has seven membership functions and its name is the same as $P_{DC\ Bus}$. The FLC rules are shown in Table 3. Based on Table 4, the capacity of each battery is 400 Ah, so the BESS capacity is 800 Ah. The total power that can be supplied to the load is 38.4 kWh, while the total voltage of the battery connected in series and parallel is 48 V. This voltage is the BESS voltage.

Based on Fig. 13, the Microgrid is represented as a single-phase (220 V) AC power grid. The 2 KW solar power plant (PVA1) is a major renewable energy source. The power sources are system power, solar power generation, and storage batteries (48 V, 800 Ah). The storage battery is controlled by a battery controller, based on fuzzy logic and it absorbs excess power if there is excess power or supplies insufficient power if there is a shortage of power in the network (AC bus). Two ordinary houses consume power as an electric load, with a capacity of 1.5 KW. The microgrid is connected to the AC bus (PV connected to the network) at a network voltage of 220 V AC. This network voltage is the PLN network voltage, from the distribution transformer (20 KV / 220 V).

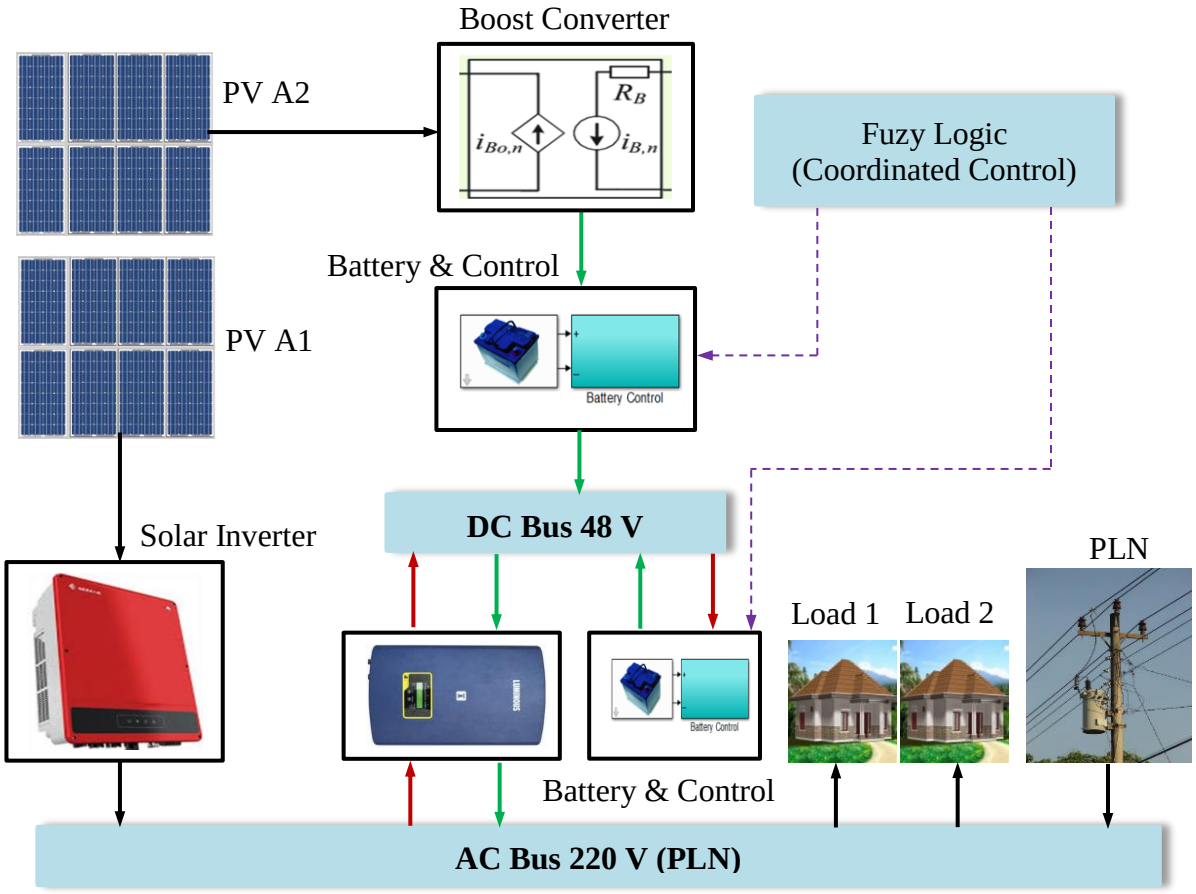

Figure. 13 Modified the AC coupling configuration

7. Results and discussions

7.1 Microgrid system operation

In a microgrid study with modified AC coupling configuration was carried out in Semarang, Indonesia, on October 28, 2020. In October it has solar radiation of KW /m2. The city of Semarang has the potential for the development of power plants using solar energy. This is in accordance with Table 5 data, solar radiation data in 2020.

Table 5. Radiation data for the city of semarang, 2020

Month	Irradiance (KW/m^2)
January	23738.75
February	31986.60
March	29139.63
April	30479.38
May	34582.37
June	35252.25
July	35126.64
August	36047.73
September	34540.51
October	33200.75
November	33703.16
December	28804.69

Table 6. Parameters in microgrid studies

Parameter	Value
Rated AC bus voltage	220 V
Rated DC bus voltage	48 V
Maximum output power of PLN network	1 KW
Maximum output power of PVA1	2 KW
Maximum output power of PVA2	1 KWp
BESS 1	9.6 KWh
BESS 2	9.6 KWh
Load 1	0.75 KW
Load 2	0.75 KW

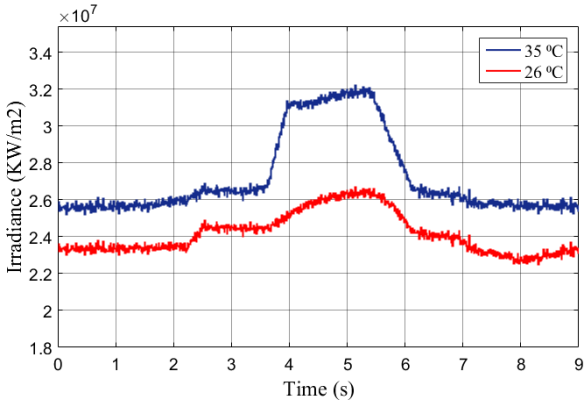

Figure. 14 Solar radiation of Semarang, 28 October 2020

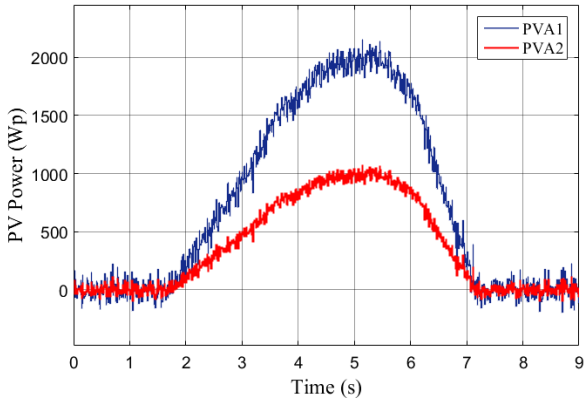

Figure. 15 PVA1 and PVA2 output power

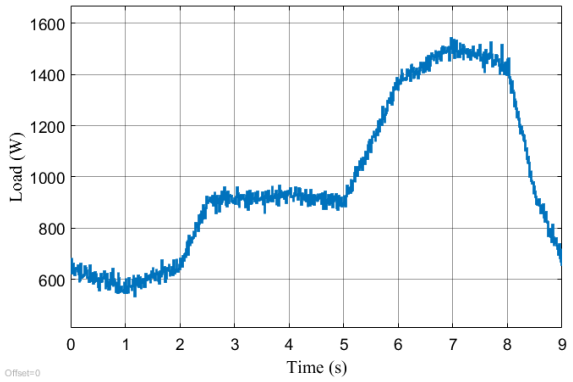

Figure. 16 Residential load

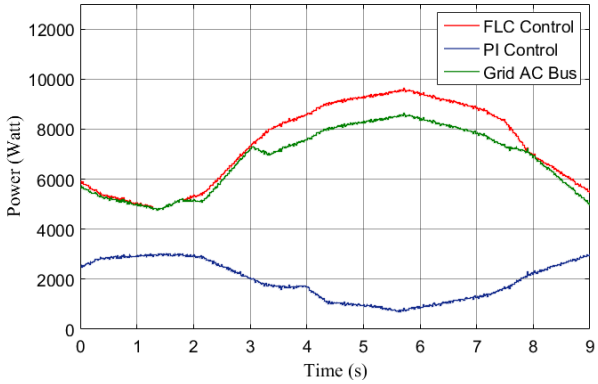

Figure. 17 BESS output power and grid power

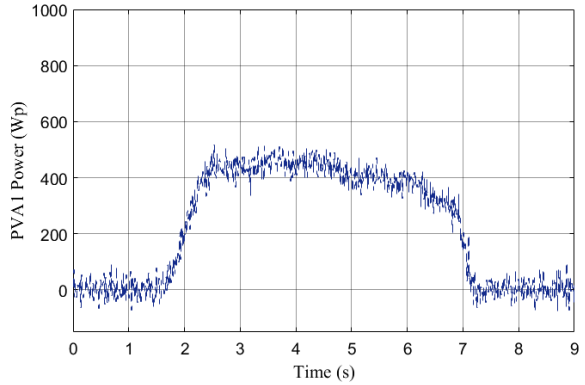

Figure. 18 Decrease in the output power of PVA1

Table 6 shows the parameters used in this microgrid study, using Matlab. The battery energy storage system (BESS) consists of BESS 1 and BESS 2. BESS 1 is an arrangement of batteries connected in series and parallel, used to store excess energy from the AC bus grid, while BESS 2 is used to store energy from PVA2. Fig. 14 shows the effect of temperature on changes in the intensity of solar radiation. In this microgrid system used PV Array 1 (PVA1) 2000 Wp and PV Array 2 (PVA2) of 1000 Wp, Fig. 15. To test the system performance used solar radiation intensity of 1000 W/m2. The MPPT used automatically extracts the maximum power from the PVA1. At start (0 seconds), MPPT will start working and PV array 1 provides power for the solar inverter and PV array 2 provides power to be stored in BESS 2 via boost converter. At any one time 5 seconds the PVA1 will provide maximum power to the AC bus grid via the solar inverter, and in between 5 seconds to 9 seconds the PVA1 will provide the minimum output power.

The initial operation of the microgrid uses solar energy, in this case the PVA1 is connected to the power grid via a solar inverter. The load on this microgrid uses a housing load with a capacity of 750 watts, so if the load is two houses, the load capacity is 1500 watts. When load 1 and load 2 are connected to the network, the AC bus grid load increases, at 5 seconds to 8 seconds it reaches peak load, Fig. 16.

7.2 PV connected grid

The purpose of the PV connected to the AC bus grid is to provide energy from the PVA1 to the grid using a solar inverter. When the solar irradiance is maximum, the power supplied to the grid is 2000 watts, while the power from the PLN network is 1000 watts, so the total power on the grid is 3000 watts, as shown in Fig. 17, when the time is 1 second to 2 seconds.

When there is a decrease in solar irradiance, the output power of PVA1 will also decrease, in Fig. 17 when the time is 2 seconds to 7 seconds, the power on the grid decreases. Likewise in Fig. 18 when the time from 2 seconds to 7 shows a decrease in PVA1 power. Because the PVA1 output power drops, the solar inverter output voltage also drops, when within 3 seconds the solar inverter output voltage is 140 V AC, shown in Fig. 19. In this study, the solar inverter used has an input voltage of 48 V DC with a capacity of 3 KW. Whereas the battery inverter uses a 4 KW bidirectional inverter with an input voltage of 48 V DC, a carrier frequency of 1950 Hz and with a base frequency of 50 Hz. The active current reference id is specified for the PVA1 DC voltage. Based on the

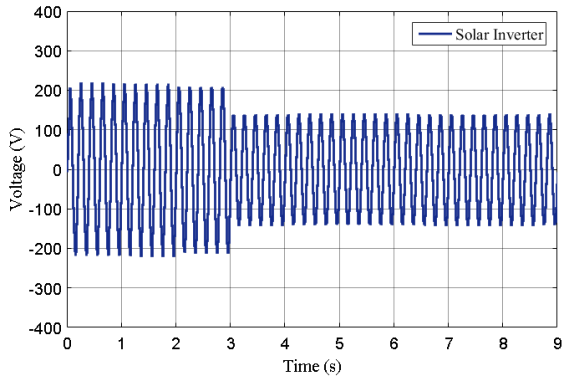

Figure. 19 The output voltage of the solar inverter

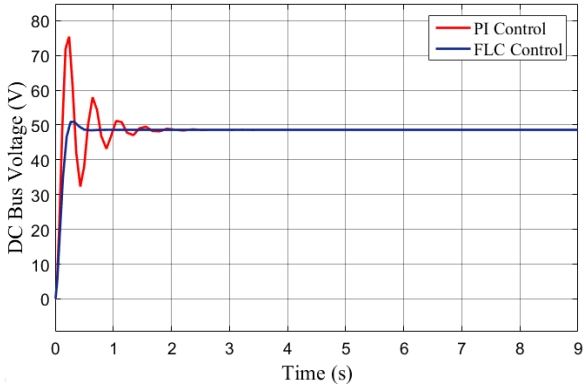

Figure. 20 Response control BESS

Table 7. Response time to BESS control strategy

Controller	Rise time (s)	Settling time (s)	Overshoot (%)
FLC	1.85	14.04	4.73
PI	1.81	26.29	55.14

reference current Id and Iq (reactive current), the PVA1 DC output voltage as the required reference voltage for the inverter, the reference Iq is set to zero.

The inverter PWM generator generates a switching signal to the IGBT based on the required reference voltage. Because there is a change in the output power of PVA1, the energy stored in the BESS will be supplied to the grid using an inverter battery. The main objective of the BESS battery control strategy is to stabilize the output power on the AC bus grid. With times ranging from 2 seconds to 7 seconds, the microgrid system works using the energy stored in the BESS. In this mode, BESS will provide output power with SOC above 50, Fig. 17. The BESS battery control strategy uses fuzzy logic (FLC) control compared to PI control.

Fig. 20 shows a graph of the DC bus voltage supplied from the BESS battery. Based on the graph, it can be seen that the fuzzy logic (FLC) control strategy shows better characteristics when compared to using PI control. Fuzzy logic control shows lower overshoot and settling time, when compared to PI control. In addition, the DC bus voltage becomes

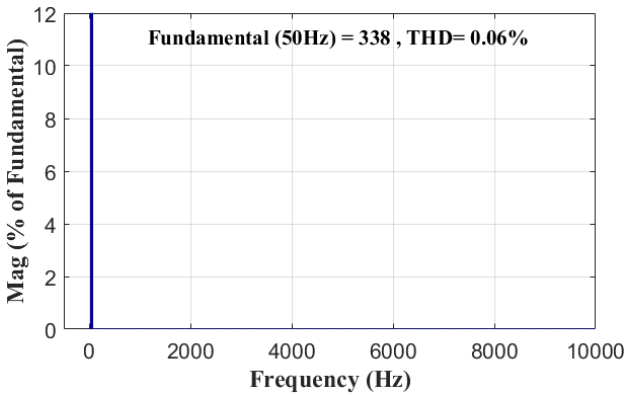

Figure. 21 Harmonic spectrum of the AC bus voltage

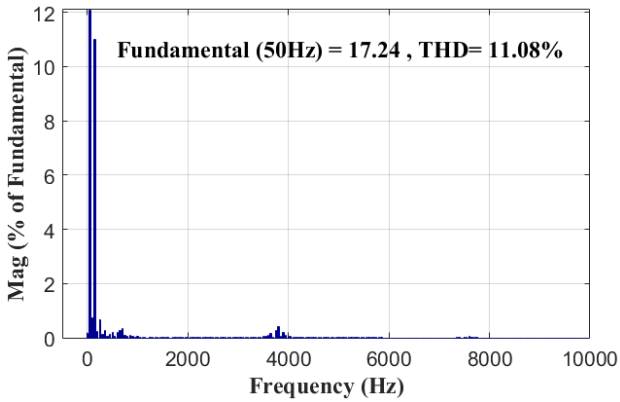

Figure. 22 Harmonic spectrum of current

stable with fuzzy logic control. Table 7 shows the response time data for the control strategy used in adjusting the DC bus voltage so that it is stable at 48 V.

The voltage on the AC bus network is kept constant as long as there is a change in load and the current on the network will change according to changes in the amount of load in the residence. In PV connected grid mode the THD voltage and current on the AC grid bus are 0.06% and 11.08%, as shown in Fig. 21 and Fig. 22.

7.3 Mode Island

When there is no solar energy or Semarang city in cloudy and rainy weather, the microgrid system works in island mode. In this mode the energy stored in the BESS is used to supply power to the grid using an inverter battery. Fig. 23 shows the BESS output power supplied to the DC bus. From the DC bus the power is supplied to the grid using an inverter battery. Fuzzy logic control strategy (FLC) was compared with PI control. Fuzzy logic control is able to regulate the power output of BESS1 and BESS 2, so that at 2.3 seconds the BESS power increases due to an increase in load. While the PI control at 4.4 seconds experienced an increase in BESS power. Therefore,

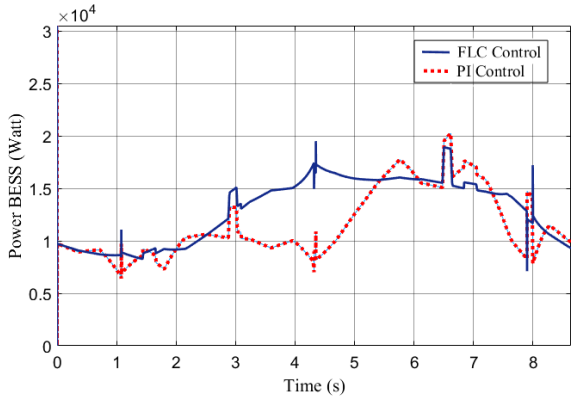

Figure. 23 BESS mode island output power

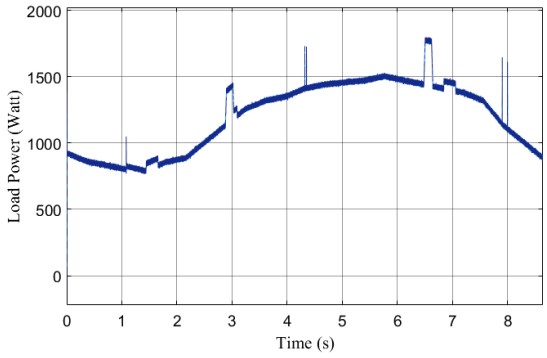

Figure. 24 Load power on island mode

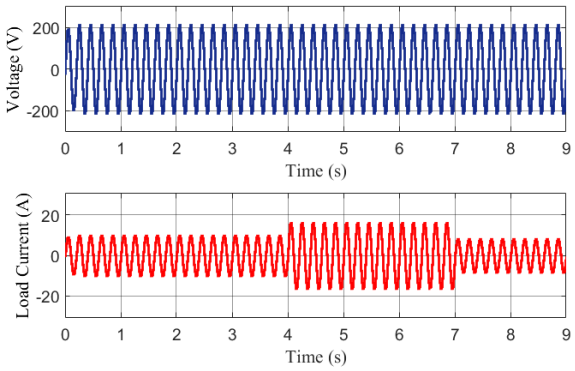

Figure. 25 Voltage and current changes on the AC grid bus

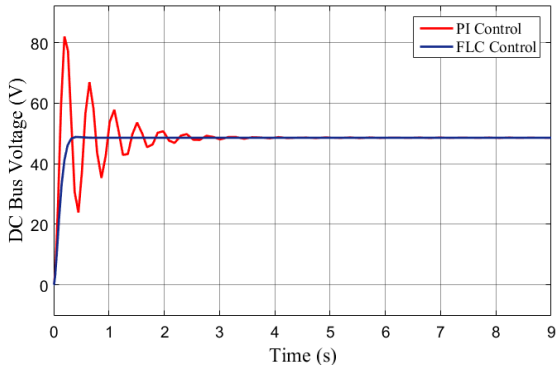

Figure. 26 Response time of BESS control

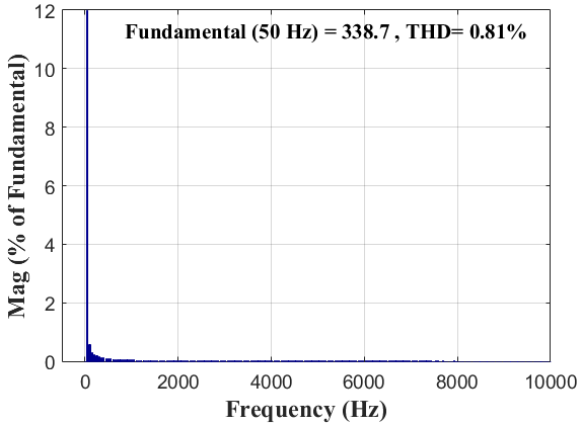

Figure. 27 Harmonic spectrum of the AC bus voltage, mode island

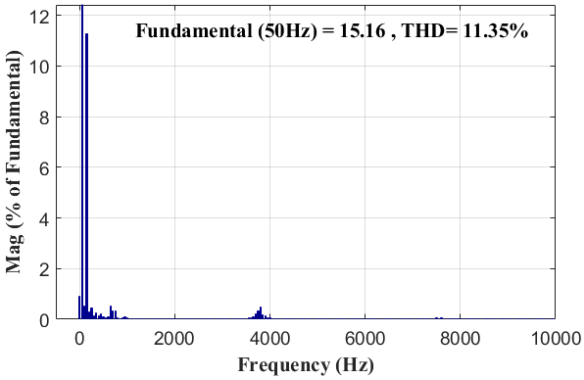

Figure. 28 Harmonic spectrum of current, mode island

Table 8. Response time on island mode BESS control

Controller	Rise time (s)	Settling time (s)	Overshoot (%)
FLC	1.68	13.78	0.54
PI	1.64	38.11	68.78

PI control is slower in meeting load power requirements when compared to fuzzy logic control.

Fig. 24 shows the load change at 2.3 seconds, while Fig. 25 shows the load voltage and current on the AC bus grid.

Fig. 26 shows the time response of the DC bus voltage graph supplied from the BESS battery using fuzzy logic (FLC) control and PI control. Based on the graph, it can be seen that the fuzzy logic (FLC) control strategy shows better performance when compared to using PI control. Fuzzy logic control shows an overshoot of 0.54% and a lower settling time of 13.78, when compared to PI control, Table 3.

Therefore, the DC bus voltage becomes stable with fuzzy logic control. Likewise, Fig. 27 and 28 show the low voltage and current THD in island mode, namely 0.8% for voltage THD and 11.35% for current THD. Therefore, the modified configuration of the AC coupling is very effective in increasing the

microgrid system for large capacities in serving residential load power.

8. Conclusion

A coordinated control scheme based on fuzzy logic on the BESS (battery energy storage system) was developed for microgrids with a modified AC coupling configuration. The coordinated control scheme in BESS is to reduce the fluctuation of active power from the microgrid when the PV is connected to the grid. In addition, this coordinated control scheme is able to provide stable power and voltage to the AC bus grid when it is not connected to the network or island operation. With a stable voltage, the frequency on the grid is also stable. It also appears that the SOC level affects the performance of BESS. The study results show that the transients that occur at the BESS voltage output can be minimized by using an FLC controller compared to a PI controller. Likewise, the BESS output power is better at delivering to the load when compared to the PI controller. When an FLC based controller is used to control the BESS it increases the response of the BESS system and reduces the voltage fluctuation on the DC bus.

Author Contributions

Conceptualization, A. Kusmantoro; methodology, A. Kusmantoro, and V. Lystianingrum; software, A. Kusmantoro; validation, A. Kusmantoro, V. Lystianingrum, A. Priyadi, and M.H. Purnomo; formal analysis, A. Kusmantoro, V. Lystianingrum, A. Priyadi, and M.H. Purnomo; investigation, A. Kusmantoro, V. Lystianingrum, A. Priyadi, and M.H. Purnomo; resources, A. Kusmantoro, and V. Lystianingrum; data curation, A. Kusmantoro, and V. Lystianingrum; writing—original draft preparation, A. Kusmantoro; writing—review and editing, A. Kusmantoro, and V. Lystianingrum; visualization, A. Kusmantoro; supervision, A. Priyadi, and M.H. Purnomo; project administration, A. Kusmantoro. All authors read and approved the final manuscript.

Acknowledgments

This work is supported by the Laboratory of Measurement Instrumentation and Identification Power System (LIPIST) in the Department of Electrical Engineering, Faculty of Electrical and Intelligent Information Technology at Institut Teknologi Sepuluh Nopember Surabaya.

References

[1] V. Lavanya and N. Senthil Kumar, "A Review: Control Strategies for Power Quality Improvement in Microgrid", *International Journal of Renewable Energy Research*, Vol. 8, No. 1, pp. 150-165, 2018.

[2] D. R. Aryani and H. Son, "Coordination Control Strategy For AC/DC Hybrid Microgrids In Stand-Alone Mode", *Energies*, Vol. 9, No. 6, pp. 1-20, 2016.

[3] H. Zhao, Q. Wu, C. Wang, L. Cheng, C. N. Rasmussen, "Fuzzy Logic Based Coordinated Control Of Battery Energy Storage System And Dispatchable Distributed Generation For Microgrid", *Journal of Modern Power Systems and Clean Energy*, Vol. 3, No. 3, pp. 422–428, 2015.

[4] M. Rashad, U. Raoof, M. Ashraf, and B. A. Ahmed, "Proportional Load Sharing and Stability of DC Microgrid with Distributed Architecture Using SM Controller", *Mathematical Problems in Engineering*, Vol. 1, No. 1, pp. 1-16, 2018.

[5] N. P. Tulasi and L. D. Aithepalli, "Droop Control of Bi-Directional DC-DC Converter for Improved Voltage Regulation and Load Sharing in DC Microgrid", *International Journal of Intelligent Engineering and Systems*, Vol. 12, No. 3, pp. 228-243, 2019.

[6] N. Eghtedarpour, "A Synergetic Control Architecture for The Integration of Photovoltaic Generation and Battery Energy Storage in DC Microgrids", *Sustainable Energy, Grids and Networks*, Vol. 20, No. 6, pp. 1-9, 2019.

[7] M. A. Eltawil and Z. Zhao, "Grid-Connected Photovoltaic Power Systems: Technical and Potential Problems - A Review", *Renewable and Sustainable Energy Reviews*, Vol. 14, No. 1, pp. 112–129, 2010.

[8] K. Srikumar and C. H. Saibabu, "A System and Novel Methodology to Track Maximum Power from Photovoltaic System: A Comparative and Experimental Analysis", *Journal of King Saud University – Engineering Sciences*, Vol. 32, No. 7, pp. 442-458, 2020.

[9] E. Cuce, P. M. Cuce, T. Bali, "An Experimental Analysis of Illumination Intensity and Temperature Dependency of Photovoltaic Cell Parameters", *Applied Energy*, Vol. 111, No. 3, pp. 374-382, 2013.

[10] X. Zhang, Q. Gao, Z. Guo, H. Zhang, M. Li1, and F. Li, "Coordinated Control Strategy for A PV-Storage Grid Connected System Based on A

Virtual Synchronous Generator", *Global Energy Interconnection*, Vol. 3, No. 1, pp. 51-59, 2020.

[11] N. Khan, M. Aamir, F. Mehmood, M. Aslam, M. Arif, "Design of Grid-Connected Photovoltaic System", *Journal of Power and Energy Engineering*, Vol. 5, No. 8, pp. 1-12, 2017.

[12] Amirullah, Adiananda, O. Penangsang, and A. Soeprijanto, "Load Active Power Transfer Enhancement Using UPQC-PV-BES System with Fuzzy Logic Controller", *International Journal of Intelligent Engineering and Systems*, Vol. 13, No. 2, pp. 329-349, 2020.

[13] P. S. Sikder, N. Pal, "Modeling of an Intelligent Battery Controller for Standalone Solar-Wind Hybrid Distributed Generation System", *Journal of King Saud University – Engineering Sciences*, Vol. 32, No. 6, pp. 368-377, 2020.

[14] J. A. R. Hernanz, J. J. Campayo, J. Laranaga, E. Zulueta, O. Barambones, J. Motrico, U.F. Gamiz, I. Zamora, "Two Photovoltaic Cell Simulation Models in Matlab/ Simulink", *International Journal on Technical and Physical Problems of Engineering*, Vol. 4, No. 1, pp. 45-51, 2012.

[15] B. Bhandari, S. R. Poudel, K. T. Lee, S. H. Ahn, "Mathematical modeling of hybrid renewable energy system: A review on small hydro-solar-wind power generation", *International Journal of Precision Engineering and Manufacturing - Green Technology*, Vol. 1, No. 2, pp. 157-173, 2014.

[16] S. Hong, J. Bae, B. Koo, I. Chang, G.Y. Cho, Y.B. Kim, S.W. Cha, F.B. Prinz, "Nanostructuring Methods for Enhancing Light Absorption Rate of Si-based Photovoltaic Devices: A review", *International Journal of Precision Engineering and Manufacturing-Green Technology*, Vol. 1, No. 1, pp. 67-74, 2014.

[17] L. Ye, H. B. Sun, X. R. Song, and L.C. Li, "Dynamic Modeling of a Hybrid Wind/ Solar/ Hydro Microgrid in EMTP/ATP", *Renewable Energy*, Vol. 39, No.1, pp. 96-106, 2012.

[18] A. Keyhani, A. Chatterjee, "Automatic Generation Control Structure For Smart Power Grids", *IEEE Transactions on Smart Grid*, Vol. 3 , No. 3, pp. 1310 – 1316, 2011.

[19] W. Zhou, H. Yang, and Z. Fang, "A Novel Model for Photovoltaic Array Performance Prediction", *Applied Energy*, Vol. 84, No. 12, pp. 1187-1198, 2007.

[20] N. Agarwal, A. Kumar, and V. Goel, "Optimization of Grid Independent Hybrid PV–Diesel–Battery System for Power Generation In Remote Villages Of Uttar Pradesh India", *Energy for Sustainable Development*, Vol. 17, No. 3, pp. 210-219, 2013.

[21] A. K. Daud and M. S. Ismail, "Design of Isolated Hybrid Systems Minimizing Costs and Pollutant Emissions", *Renewable Energy*, Vol. 44, No. 3, pp. 215–224, 2012.

[22] B. G. Sujatha and G. S. Anitha, "Enhancement of PQ In Grid Connected PV System Using Hybrid Technique", *Ain Shams Engineering Journal*, Vol. 9, No. 4, pp. 869-881, 2018.

[23] Y. Yongheng and B. Frede, "Low-Voltage Ride-Through Capability of a Single-Stage Single-Phase Photovoltaic System Connected to The Low-Voltage Grid", *International Journal of Photoenergy*, Vol. 1, No. 1, pp. 1–9, 2013.

[24] A. M. Humada, M. Hojabri, M. Herwan, H. M. Hamada, and M. N. Ahmed, "Photovoltaic Grid-Connected Modeling and Characterization Based On Experimental Results", *Journal Plos One*, Vol. 11, No. 4, pp. 1-13, 2016.

[25] U. B. Tayab and M. Kashif1, "A Modified Droop Controller for Parallel Operation of Single-Phase Inverters In Islanded Microgrid", *International Journal of Intelligent Engineering and Systems*, Vol. 10, No. 4, pp. 11-17, 2017.

[26] A. H. M. Nordin, A. M. Omar, and H. Zainuddin, "Modeling and Simulation of Grid Inverter in Grid Connected Photovoltaic System", *International Journal of Renewable Energy Research*, Vol. 4, No. 4, pp. 949-957, 2014.

[27] M. A. Omar and M. Mahmoud, "Design and Simulation of a PV System Operating in Grid-Connected and Stand-Alone Modes for Areas of Daily Grid Blackouts", *International Journal of Photoenergy*, Vol. 1, No. 1, pp. 1-9, 2019.

[28] K. Karabacak and N. Cetin, "Artificial Neural Networks for Controlling Wind-PV Power Systems: A review", *Renewable and Sustainable Energy Reviews*, Vol. 29, No. 1, pp. 804-827, 2014.

[29] M. R. Aghamohammadi and H. Abdolahinia, "A New Approach for Optimal Sizing of Battery Energy Storage System for Primary Frequency Control of Islanded Microgrid", *International Journal Electrical Power Energy System*, Vol. 54, No. 1, pp. 325–333, 2014.

[30] D. Wu, F. Tang, T. Dragicevic, J. C. Vasquez, and J. M. Guerrero, "Autonomous Active Power Control for Islanded AC Microgrids with Photovoltaic Generation and Energy Storage System", *IEEE Transaction on Energy Conversion*, Vol. 9, No. 4, pp. 882–892, 2014.